



# Discovery of an Ultra-faint Stellar System near the Magellanic Clouds with the DECam Local Volume Exploration Survey

W. Cerny<sup>1,2,3</sup> , A. B. Pace<sup>4</sup> , A. Drlica-Wagner<sup>1,2,3</sup> , P. S. Ferguson<sup>5,6</sup> , S. Mau<sup>7,8</sup> , M. Adamów<sup>9</sup> , J. L. Carlin<sup>10</sup> , Y. Choi<sup>11</sup> , D. Erkal<sup>12</sup> , L. C. Johnson<sup>13</sup> , T. S. Li<sup>14,15,28</sup> , C. E. Martínez-Vázquez<sup>16</sup> , B. Mutlu-Pakdil<sup>1,2</sup> , D. L. Nidever<sup>17,18</sup> , K. A. G. Olsen<sup>18</sup> , A. Pieres<sup>19,20</sup> , E. J. Tollerud<sup>11</sup> , J. D. Simon<sup>14</sup> , A. K. Vivas<sup>16</sup> , D. J. James<sup>21</sup> , N. Kuropatkin<sup>3</sup> , S. Majewski<sup>22</sup> , D. Martínez-Delgado<sup>23</sup> , P. Massana<sup>12</sup> , A. E. Miller<sup>24</sup> , E. H. Nielsen<sup>3</sup> , N. E. D. Noël<sup>12</sup> , A. H. Riley<sup>5,6</sup> , D. J. Sand<sup>25</sup> , L. Santana-Silva<sup>26</sup> , G. S. Stringfellow<sup>27</sup> , and D. L. Tucker<sup>3</sup>

(DELVE Collaboration)

<sup>1</sup> Kavli Institute for Cosmological Physics, University of Chicago, Chicago, IL 60637, USA; [williamcerny@uchicago.edu](mailto:williamcerny@uchicago.edu)

<sup>2</sup> Department of Astronomy and Astrophysics, University of Chicago, Chicago, IL 60637, USA

<sup>3</sup> Fermi National Accelerator Laboratory, P.O. Box 500, Batavia, IL 60510, USA

<sup>4</sup> McWilliams Center for Cosmology, Carnegie Mellon University, 5000 Forbes Avenue, Pittsburgh, PA 15213, USA; [apace@andrew.cmu.edu](mailto:apace@andrew.cmu.edu)

<sup>5</sup> George P. and Cynthia Woods Mitchell Institute for Fundamental Physics and Astronomy, Texas A&M University, College Station, TX 77843, USA

<sup>6</sup> Department of Physics and Astronomy, Texas A&M University, College Station, TX 77843, USA

<sup>7</sup> Department of Physics, Stanford University, 382 Via Pueblo Mall, Stanford, CA 94305, USA

<sup>8</sup> Kavli Institute for Particle Astrophysics & Cosmology, P.O. Box 2450, Stanford University, Stanford, CA 94305, USA

<sup>9</sup> National Center for Supercomputing Applications, University of Illinois, 1205 West Clark Street, Urbana, IL 61801, USA

<sup>10</sup> Rubin Observatory/AURA, 950 North Cherry Avenue, Tucson, AZ 85719, USA

<sup>11</sup> Space Telescope Science Institute, 3700 San Martin Drive, Baltimore, MD 21218, USA

<sup>12</sup> Department of Physics, University of Surrey, Guildford GU2 7XH, UK

<sup>13</sup> Center for Interdisciplinary Exploration and Research in Astrophysics (CIERA) and Department of Physics and Astronomy, Northwestern University, 1800 Sherman Avenue, Evanston, IL 60201, USA

<sup>14</sup> Observatories of the Carnegie Institution for Science, 813 Santa Barbara Street, Pasadena, CA 91101, USA

<sup>15</sup> Department of Astrophysical Sciences, Princeton University, Princeton, NJ 08544, USA

<sup>16</sup> Cerro Tololo Inter-American Observatory, NSF's National Optical-Infrared Astronomy Research Laboratory, Casilla 603, La Serena, Chile

<sup>17</sup> Department of Physics, Montana State University, P.O. Box 173840, Bozeman, MT 59717-3840, USA

<sup>18</sup> NSF's National Optical-Infrared Astronomy Research Laboratory, 950 North Cherry Avenue, Tucson, AZ 85719, USA

<sup>19</sup> Laboratório Interinstitucional de e-Astronomia—LINEA, Rua Gal. José Cristino 77, Rio de Janeiro, RJ—20921-400, Brazil

<sup>20</sup> Observatório Nacional, Rua Gal. José Cristino 77, Rio de Janeiro, RJ—20921-400, Brazil

<sup>21</sup> ASTRAVEO, LLC, P.O. Box 1668, Gloucester, MA 01931, USA

<sup>22</sup> Department of Astronomy, University of Virginia, Charlottesville, VA 22904, USA

<sup>23</sup> Instituto de Astrofísica de Andalucía, CSIC, E-18080 Granada, Spain

<sup>24</sup> Leibniz-Institut für Astrophysik Potsdam (AIP), An der Sternwarte 16, D-14482 Potsdam, Germany

<sup>25</sup> Department of Astronomy/Steward Observatory, 933 North Cherry Avenue, Room N204, Tucson, AZ 85721-0065, USA

<sup>26</sup> NAT-Universidade Cruzeiro do Sul/Universidade Cidade de São Paulo, Rua Galvão Bueno, 868, 01506-000, São Paulo, SP, Brazil

<sup>27</sup> Center for Astrophysics and Space Astronomy, University of Colorado, 389 UCB, Boulder, CO 80309-0389, USA

Received 2020 September 17; revised 2021 January 29; accepted 2021 January 30; published 2021 March 23

## Abstract

We report the discovery of a new ultra-faint stellar system found near the Magellanic Clouds in the DECam Local Volume Exploration Survey. This new system, DELVE J0155–6815 (DELVE 2), is located at a heliocentric distance of  $D_{\odot} = 71 \pm 4$  kpc, which places it at a 3D physical separation of  $12 \pm 3$  kpc from the center of the Small Magellanic Cloud and  $28^{+4}_{-3}$  kpc from the center of the Large Magellanic Cloud (LMC). DELVE 2 is identified as a resolved overdensity of old ( $\tau > 13.3$  Gyr) and metal-poor ( $[Fe/H] = -2.0^{+0.2}_{-0.5}$  dex) stars with a projected half-light radius of  $r_{1/2} = 21^{+4}_{-3}$  pc and an absolute magnitude of  $M_V = -2.1^{+0.4}_{-0.5}$  mag. The size and luminosity of DELVE 2 are consistent with both the population of recently discovered ultra-faint globular clusters and the smallest ultra-faint dwarf galaxies. However, its photometrically derived age and metallicity would place it among the oldest and most metal-poor globular clusters in the Magellanic system. In the absence of spectroscopic measurements of the system's metallicity dispersion and internal kinematics, we are unable to conclusively classify this system at this time. DELVE 2 is detected in *Gaia* DR2 with a clear proper-motion signal, with multiple blue horizontal-branch stars near the centroid of the system with proper motions consistent with the systemic mean. We measure the system proper motion to be  $(\mu_{\alpha} \cos \delta, \mu_{\delta}) = (1.02^{+0.24}_{-0.25}, -0.85^{+0.18}_{-0.19})$  mas yr<sup>-1</sup>. We compare the spatial position and proper motion of DELVE 2 with simulations of the accreted satellite population of the LMC and find that it is very likely to be associated with the LMC.

*Unified Astronomy Thesaurus concepts:* Dwarf galaxies (416); Local Group (929); Star clusters (1567); Milky Way Galaxy (1054); Magellanic Clouds (990)

<sup>28</sup> NHFP Einstein Fellow.

## 1. Introduction

The advent of large-scale digital sky surveys has revolutionized our understanding of the Milky Way and its satellite system. In particular, systematic searches of the Northern Hemisphere sky conducted with the Sloan Digital Sky Survey (SDSS; York et al. 2000) first illuminated the Milky Way’s lowest surface brightness populations, doubling the number of known dwarf galaxy satellites (e.g., Willman et al. 2005a, 2005b; Belokurov et al. 2006, 2007, 2009, 2010; Zucker et al. 2006a, 2006b). The Pan-STARRS-1 (PS1; Chambers et al. 2016) survey has further increased the coverage and depth of Northern Hemisphere surveys, resulting in the discovery of several new ultra-faint systems (e.g., Laevens et al. 2014, 2015a, 2015b). Furthermore, the advent of the Dark Energy Camera (DECam; Flaugher et al. 2015) on the 4 m Blanco Telescope at the Cerro Tololo Inter-American Observatory in Chile has resulted in the discovery of a multitude of faint satellite galaxies and compact star clusters orbiting the Milky Way at surface brightnesses inaccessible to previous photographic surveys and SDSS. The DECam searches covering  $\sim 5000 \text{ deg}^2$  of the southern sky using data from the Dark Energy Survey (DES; DES Collaboration et al. 2005, 2016) resulted in the discovery of more than 20 new star cluster and dwarf galaxy satellites (e.g., Bechtol et al. 2015; Drlica-Wagner et al. 2015; Kim & Jerjen 2015a; Koposov et al. 2015a; Luque et al. 2016, 2018). These efforts have continued through a number of recent community-led DECam surveys, including the Survey of the MAGellanic Stellar History (SMASH; e.g., Martin et al. 2015; Nidever et al. 2017), the Magellanic Satellites Survey (MagLiteS; e.g., Drlica-Wagner et al. 2016; Torrealba et al. 2018), and the Magellanic Edges Survey (e.g., Koposov et al. 2018), all of which have contributed to the census of Milky Way satellites, especially in the region of sky in the periphery of the Magellanic Clouds. In addition, several other surveys have found new ultra-faint dwarf galaxies, including the Hyper Suprime-Cam Survey (Homma et al. 2016, 2018, 2019), VST ATLAS (Torrealba et al. 2016a, 2016b), and *Gaia* (Torrealba et al. 2019).

The detection of a large number of ultra-faint satellites ( $\sim 30$  in total) proximate to the Large and Small Magellanic Clouds (LMC and SMC, respectively) has contributed to a growing body of theoretical and observational evidence suggesting that the LMC and SMC have brought their own satellite populations into the Milky Way (e.g., Lynden-Bell 1976; D’Onghia & Lake 2008; Deason et al. 2015; Dooley et al. 2017; Sales et al. 2017; Jethwa et al. 2018; Kallivayalil et al. 2018; Erkal & Belokurov 2020; Jahn et al. 2019; Nadler et al. 2020; Patel et al. 2020). In fact, the spatial distribution of the dwarf galaxy satellites discovered in the DES footprint alone excludes an isotropic spatial distribution for the Milky Way satellites at the  $>3\sigma$  level (Bechtol et al. 2015; Drlica-Wagner et al. 2015; Koposov et al. 2015a; Sales et al. 2017; Fritz et al. 2018). Furthermore, high-precision proper-motion measurements from the *Gaia* satellite (Gaia Collaboration et al. 2018), combined with radial velocity measurements, have allowed for the determination of these systems’ 3D kinematics and orbital histories, linking some dwarf galaxies and star clusters to the Magellanic system (e.g., Kallivayalil et al. 2018; Patel et al. 2020).

This developing picture of the Magellanic satellite system offers important insight into the  $\Lambda$ CDM paradigm, which predicts that galaxies form hierarchically across a wide range of mass scales. Furthermore, these low-mass, low surface brightness substructures can provide a wealth of

information about their host halos—in this case, the Magellanic Clouds. For example, these satellites have been used to place stringent constraints on the LMC/SMC mass (Erkal & Belokurov 2020) and, through comparison with cosmological simulations, trace the orbital history of the Clouds themselves (e.g., Deason et al. 2015; Jethwa et al. 2016).

In this work, we present the discovery of an old, metal-poor, ultra-faint system, DELVE J0155–6815 (DELVE 2), in the vicinity of the Magellanic Clouds. In addition to being a newly discovered member of the scarce population of old Magellanic stellar systems, this new system also occupies a region of size–magnitude space that makes it difficult to classify as either an ultra-faint cluster or a dwarf galaxy. Due to this classification ambiguity, we refer to this new system as DELVE 2 throughout this work and consider several potential methods for elucidating the true nature of the system.

This paper is structured as follows. In Section 2, we describe the DECam Local Volume Exploration Survey (DELVE) survey observations and source catalogs used in this study. In Section 3, we detail our application of the `simple` algorithm used to search for new ultra-faint systems in the periphery of the Magellanic Clouds and present the detection of the candidate system, DELVE 2. In Section 4, we derive morphological and isochrone properties for DELVE 2 and present the detection of a clear proper-motion signal for the system in data from *Gaia* DR2. Lastly, in Section 5, we discuss the likely connection between DELVE 2 and the Magellanic system and consider how to classify DELVE 2 as a stellar system. We conclude in Section 6.

## 2. Observations and Data

The DELVE (2019A-0305) is a multicomponent, 126 night survey of the southern sky focused on studies of the satellite systems of the Milky Way, Magellanic Clouds, and several Magellanic-analog systems in the Local Volume. DELVE seeks to provide near-uniform, contiguous coverage of the southern sky with decl.  $\delta_{2000} < 0^\circ$  in the  $g$ ,  $r$ ,  $i$ , and  $z$  bands by combining all publicly available community DECam exposures with exposure times  $>30$  s with  $\sim 20,000$  new exposures in regions of the sky not previously observed by DECam. DELVE is split into three observational components: DELVE-WIDE, a wide-area ( $\sim 15,000 \text{ deg}^2$ ) survey of the high Galactic latitude southern sky to a depth of  $g \sim 23.5$  mag; DELVE-MC, a contiguous survey of the Magellanic Cloud periphery ( $\sim 2200 \text{ deg}^2$ ) to a depth of  $g \sim 24.2$  mag; and DELVE-DEEP, a deep survey to a depth of  $g \sim 25.0$  mag around four isolated Magellanic Cloud analogs in the Local Volume ( $\sim 135 \text{ deg}^2$ ), where the hierarchical prescriptions of  $\Lambda$ CDM can be tested around intermediate-mass dark matter halos.

In Mau et al. (2020), we presented results from an early satellite search over an  $\sim 4000 \text{ deg}^2$  subregion from the WIDE survey component in the northern Galactic cap bounded by  $b > 10^\circ$  and  $\delta_{2000} < 0^\circ$ .<sup>29</sup> In this work, we extend this search to a region of  $\sim 2200 \text{ deg}^2$  in the periphery of the Magellanic Clouds. Catalogs in this region were generated from community exposures and new exposures from the DELVE-WIDE and -MC survey components. Our DELVE data set was constructed of  $\sim 9000$  exposures in the periphery of the Magellanic Clouds and high Galactic latitude sky, including 1000 new exposures

<sup>29</sup> Data from this region constitute the first DELVE public data release (A. Drlica-Wagner et al. 2021, in preparation); <https://datalab.noao.edu/delve/index.php>.

from the first three semesters of DELVE observing (2019A, 2019B, and 2020A) and 8000 community exposures publicly available before 2020 April.<sup>30</sup> Broadly, we began by selecting all available exposures with exposure times between 30 and 350 s in the region of sky south of the DES footprint ( $\delta_{2000} \lesssim -60^\circ$ ). In addition, we selected regions east and west of the DES footprint at Galactic latitude  $10^\circ < b < 20^\circ$  with  $\delta_{2000} < -30^\circ$ . We further excluded exposures in the densest central regions of the LMC and SMC and removed exposures near the bright stars Canopus and  $\beta$  Carinae. The primary contributors to the selected community exposures in the region are  $\sim 3600$  exposures from MagLiteS (2016A-0366, 2018A-0242; Drlica-Wagner et al. 2016; Torrealba et al. 2018) and  $\sim 550$  exposures from SMASH (2013B-0440; Nidever et al. 2017), with other exposures sourced from more than 70 DECam observing programs. Approximately half of the selected exposures have exposure times of 90 s, consistent with the fact that DELVE-WIDE and MagLiteS performed 90 s dithered exposures in the  $g$ ,  $r$ , and  $i$  bands. The remaining exposures, while initially selected based on a cut of 30–350 s, primarily include 267 and 333 s exposures from DELVE-MC and SMASH.

We processed all exposures consistently with the DES Data Management (DESDM) pipeline (Morganson et al. 2018). This pipeline achieves subpercent-level photometric accuracy by performing full-exposure sky background subtraction (Bernstein et al. 2018) and calibrating based on custom, seasonally averaged bias and flat images. The DESDM pipeline uses `SourceExtractor` and `PSFEx` (Bertin & Arnouts 1996; Bertin 2011) on an exposure-level basis to automate source detection and photometric measurement. Stellar astrometry was calibrated against *Gaia* DR2 (Gaia Collaboration et al. 2018), which provides 30 mas astrometric precision. We calibrated the DELVE photometry by matching stars in each CCD to the ATLAS-Refcat2 catalogs (Tonry et al. 2018), which consist of measurements from PS1 DR1 (Chambers et al. 2016) and SkyMapper (Wolf et al. 2018) brought onto the PS1 filter system. Photometric measurements from this catalog were transformed to the DECam  $g$ ,  $r$ ,  $i$ , and  $z$  filters before calibration using the following equations:

$$\begin{aligned} g_{\text{DECam}} &= g_{\text{PS1}} + 0.0994(g_{\text{PS1}} - r_{\text{PS1}}) - 0.0319, \\ r_{\text{DECam}} &= r_{\text{PS1}} - 0.1335(g_{\text{PS1}} - r_{\text{PS1}}) + 0.0215, \\ i_{\text{DECam}} &= i_{\text{PS1}} - 0.3407(i_{\text{PS1}} - z_{\text{PS1}}) - 0.0013, \\ z_{\text{DECam}} &= r_{\text{PS1}} - 0.2575(r_{\text{PS1}} - z_{\text{PS1}}) - 0.0201. \end{aligned}$$

The rms scatter between the measurements of bright stars from ATLAS-Refcat2 and DELVE when calculating CCD zero-points is found to have a median value of  $g$ ,  $r$ ,  $i$ ,  $z = 3.0, 2.9, 1.7, 2.5$  mmag. Furthermore, the DELVE zero-points have an rms scatter of  $\sim 10$  mmag per CCD when compared to the DES DR1 zero-points for the same CCDs (Burke et al. 2018). The DES is calibrated independently of ATLAS-Refcat2 and is found to have an absolute photometric accuracy of  $\sim 1\%$  and a relative photometric uniformity of  $\lesssim 3$  mmag when compared to *Gaia* DR2 (DES Collaboration et al. 2018; Sevilla-Noarbe et al. 2020). More detailed characterization of the DELVE photometric calibration will accompany the first DELVE public data release (A. Drlica-Wagner et al. 2021, in preparation).

<sup>30</sup> Community exposures were downloaded from the Science Archive hosted by NSF’s National Optical-Infrared Astronomy Research Laboratory: <https://astroarchive.noao.edu/>.

We built a multiband catalog of unique sources by matching source detections between the individual single-exposure catalogs following the procedure described in Drlica-Wagner et al. (2015). We cross-matched all sources detected in individual exposures using a  $1''$  matching radius.

In total, the resulting catalog spanned an area of  $\sim 2220 \text{ deg}^2$  with simultaneous coverage in  $g$  and  $r$  and  $\sim 1880 \text{ deg}^2$  with simultaneous coverage in  $g$  and  $i$ . The difference between the  $g$ ,  $r$  coverage and the  $g$ ,  $i$  coverage is due to the availability of community data in the  $r$  and  $i$  bands. We include a map of the search region, in the context of known Magellanic satellite systems, in Figure 1.

Lastly, we calculated extinction from Milky Way foreground dust for each object through a bilinear interpolation in  $(\alpha_{2000}, \delta_{2000})$  to the maps of Schlegel et al. (1998) with the rescaled normalization factor presented by Schlafly & Finkbeiner (2011), assuming  $R_V = 3.1$  and a set of coefficients  $R_\lambda = A_\lambda / E(B - V)$  derived by DES for the  $g$ ,  $r$ , and  $i$  bands:  $R_g = 3.185$ ,  $R_r = 2.140$ , and  $R_i = 1.571$  (DES Collaboration et al. 2018). Hereafter, all magnitudes quoted are corrected for interstellar extinction. We calculate the  $10\sigma$  limiting magnitude for the entire search region to be  $g \sim 23.6$ ,  $r \sim 23.3$ , and  $i \sim 22.6$  mag.

### 3. Satellite Search

#### 3.1. Methodology

We search for old, metal-poor satellite candidates in the DELVE catalog described in Section 2 using the `simple`<sup>31</sup> algorithm, which has been successfully applied for satellite searches on other DECam data sets (e.g., Bechtol et al. 2015; Drlica-Wagner et al. 2015, 2020; Mau et al. 2019), including most recently on early DELVE data in the northern Galactic cap, which resulted in the detection of the Centaurus I dwarf galaxy candidate and the DELVE 1 halo star cluster candidate (Mau et al. 2020). The `simple` algorithm uses an isochrone matched-filter approach in color–magnitude space to enhance the contrast of spatial overdensities indicative of halo substructure against foreground Milky Way field stars. Using `simple`, we performed two complementary searches, one of which utilized the  $g$  and  $r$  bands, while the other utilized the  $g$  and  $i$  bands.

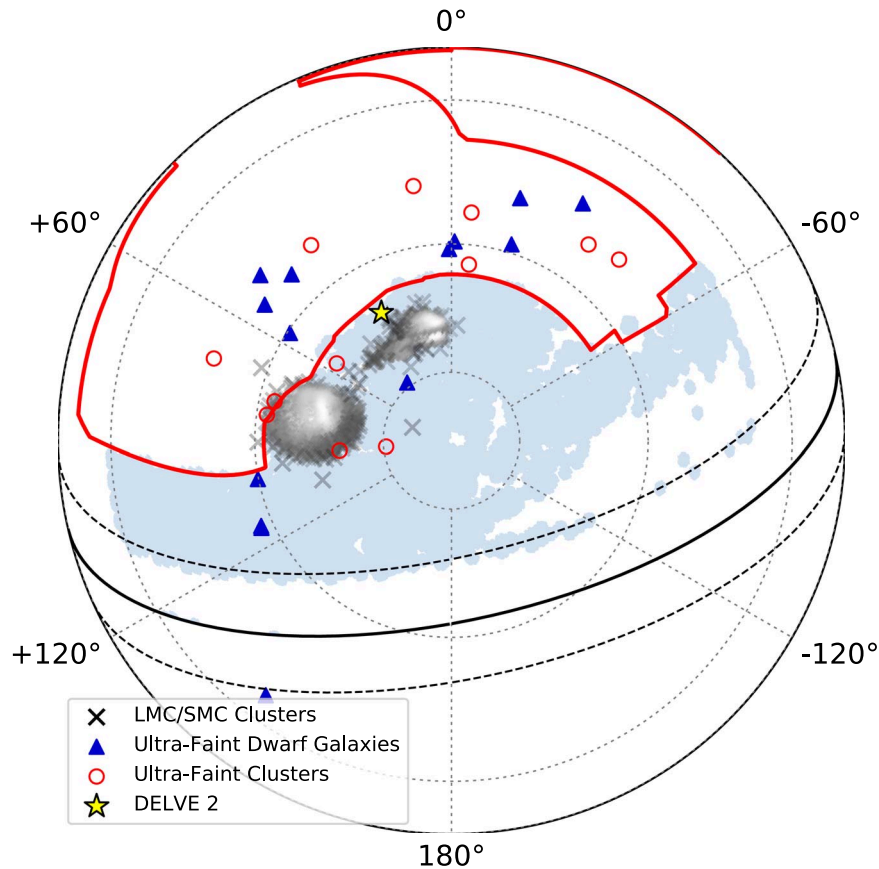
We partitioned the catalog described above into `HEALPix` (Górski et al. 2005) pixels at `nside=32`, corresponding to  $\sim 3.4 \text{ deg}^2$  pixels. For each pixel, we selected stellar objects detected in both search filters using the morphological parameter `SPREAD_MODEL` and its associated error `SPREADERR_MODEL` (Desai et al. 2012) by taking  $|\text{SPREAD\_MODEL\_R}| < 0.003 + \text{SPREADERR\_MODEL\_R}$  for the  $g$ ,  $r$ -band search and, similarly,  $|\text{SPREAD\_MODEL\_I}| < 0.003 + \text{SPREADERR\_MODEL\_I}$  for the  $g$ ,  $i$ -band search. In both cases, we also applied a magnitude selection of  $g < 23.5$  mag in order to reduce star–galaxy confusion and mitigate artificial density inhomogeneity in the data due to variations in survey depth.

After star/galaxy separation, we applied a matched-filter template using a `PARSEC` isochrone (Bressan et al. 2012) with metallicity  $Z = 0.0001$  and age  $\tau = 12 \text{ Gyr}$ .<sup>32</sup> In each

<sup>31</sup> <https://github.com/DarkEnergySurvey/simple>

<sup>32</sup> We note that for this work, we choose this template because we are specifically concerned with detecting old, metal-poor stellar systems. Drlica-Wagner et al. (2020) found that using search isochrones of different ages  $> 10 \text{ Gyr}$  did not significantly affect detection efficiency. We defer a search for younger, more metal-rich satellites of the LMC/SMC to a later work using more complete data from the DELVE-MC survey component.





**Figure 1.** Orthographic sky map of the Magellanic periphery region, including a selection of known satellites of the Milky Way and Magellanic Clouds. The blue shaded regions correspond to the  $g$ -band footprint of this search; i.e., these regions encompass the total area covered by searches in both the  $g, r$  and  $g, i$  bands. The red outline corresponds to the DES footprint. The black line corresponds to a Galactic latitude of  $b = 0^\circ$ , while the dashed lines correspond to  $b = \pm 10^\circ$ . The LMC/SMC star clusters from the catalogs of Bica et al. (2008, 2020) are drawn in gray scale, with denser regions of clusters shown in whiter colors. The location of DELVE 2 is indicated with a yellow star, lying just below the southern boundary of the DES footprint. Twenty-seven recently discovered ultra-faint star clusters and dwarf galaxies with possible Magellanic origins/associations, as listed in Bica et al. (2020), are plotted as open red circles and filled blue triangles, respectively.

inside = 32 pixel and its eight neighboring pixels, we scanned our matched filter in distance modulus in the range  $16.0 \text{ mag} < m - M < 23.5 \text{ mag}$  in intervals of 0.5 mag, searching for spatial overdensities of old, metal-poor stars characteristic of halo star clusters and ultra-faint dwarf galaxies. At each distance modulus, we selected stars within 0.1 mag of the isochrone locus in color–magnitude space according to  $\Delta(g - r) < \sqrt{0.1^2 + \sigma_g^2 + \sigma_r^2}$  (for the  $g, r$  search) or  $\Delta(g - i) < \sqrt{0.1^2 + \sigma_g^2 + \sigma_i^2}$  (for the  $g, i$  search), where  $\sigma_g$ ,  $\sigma_r$ , and  $\sigma_i$  are the photometric uncertainties for the  $g$ -,  $r$ -, and  $i$ -band point-spread function (PSF) magnitude measurements, respectively. We then smoothed the filtered stellar density field with a  $2'$  Gaussian kernel and identified local stellar density peaks by iteratively increasing a density threshold until fewer than 10 disconnected peaks were detected. Lastly, for each of the identified density peaks, we computed the Poisson significance of the observed number of filtered stars relative to an annular background field and compiled a candidate list.

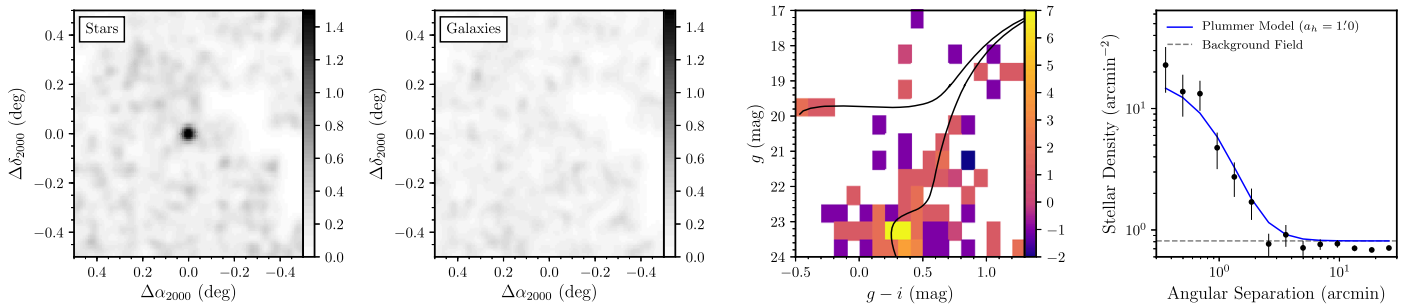
### 3.2. Detection of DELVE 2

We visually inspected diagnostic plots for all candidates identified at a Poisson significance  $\geq 5.5\sigma$  in at least one of the two searches and all candidates simultaneously identified at the  $\geq 5\sigma$  level in both searches (each of which produced fully

independent candidate lists).<sup>33</sup> In addition to recovering all known dwarf galaxies within the search footprint, including Carina (Cannon et al. 1977), Carina II and Carina III (Torrealba et al. 2018), Hydrus I (Koposov et al. 2018), Pictor II (Drlica-Wagner et al. 2016), and a number of known LMC/SMC periphery clusters, one previously unknown stellar overdensity was identified in the constellation Hydrus. This candidate, DELVE 2, was identified as a compact density peak at a Poisson significance of  $9.1\sigma$  in the  $g, r$ -band search and  $5.65\sigma$  in the  $g, i$ -band search.

In Figure 2, we present diagnostic plots for DELVE 2 similar to those inspected in the simple search results. As is visible in the two left panels, DELVE 2 was detected as a clear overdensity against the field of foreground stars (first panel) and background galaxies (second panel); however, DELVE 2 was discovered in a region of our catalog with only a single tiling in each of the  $g, r$ , and  $i$  bands, leading to a conspicuous lack of coverage to the west of the system. Our diagnostic Hess diagram (third panel) indicated a clear overdensity of main-sequence turnoff stars at the position of DELVE 2 and featured

<sup>33</sup> Initial visual inspection to remove false positives and known systems was performed by the primary author; this reduced the candidate pool to  $\sim 40$  candidates, which were subsequently analyzed by  $\sim 10$  coauthors, limiting the total remaining candidates to eight. We ran the `ugali` MCMC (Section 4) over these eight candidates, which resulted in seven of these eight candidates being deemed false positives.



**Figure 2.** Stellar density, galaxy density, Hess diagram, and radial density profile plots for DELVE 2. The visual inspection of the search results employed plots similar to these. Regions of missing coverage are visible as empty (white) regions in the density fields of the two left panels. (First panel) Isochrone-filtered stellar density field convolved with a Gaussian kernel of  $1'$ . (Second panel) Isochrone-filtered background galaxy density field convolved with a Gaussian kernel of  $1'$ . (Third panel) Color-magnitude Hess diagram corresponding to all foreground stars within  $2/5$  of the centroid of DELVE 2 minus all stars in a representative background region of the same area displaced to the east of the system (so as to avoid the region of incomplete coverage). The best-fit PARSEC isochrone (derived in Section 4; Table 1) is shown in black. White space indicates bins with no stars. The densest bin, shown in yellow, corresponds to an overdensity of main-sequence turnoff stars. Multiple candidate blue horizontal-branch stars are also visible. (Fourth panel) Radial surface density profile of stars passing the isochrone filter; the errors are derived from the standard deviation of the number of stellar sources in a given annulus divided by the area of that annulus. The blue radial profile curve corresponds to the best-fit Plummer model, assuming spherical symmetry, with  $a_h = 1/0$  (see Section 4; Table 1).

several potential blue horizontal-branch stars. Lastly, the fourth panel of Figure 2 shows the radial distribution of isochrone-filtered stars with respect to the centroid of DELVE 2.

Given the large number of previously discovered stellar systems associated with the Magellanic Clouds found in the region of sky near DELVE 2, we verified the novelty of this discovery through cross-matching the coordinates of the DELVE 2 system with multiple independently maintained astronomical data sets/databases. Adopting the discovery coordinate centroid of  $(\alpha_{2000}, \delta_{2000}) = (28^\circ 77', -68^\circ 27')$ . We did not find any known stellar systems within  $10'$  in SIMBAD (Wenger et al. 2000), the catalog of known confirmed or candidate Milky Way satellite dwarf galaxies presented in Table 2 of Drlica-Wagner et al. (2020), the catalog of Magellanic Cloud star clusters and stellar associations presented by Bica et al. (2008) and its comprehensive recent update of SMC/Magellanic bridge stellar systems (Bica et al. 2020), which includes a list of 27 ultra-faint Magellanic-region systems. While the catalog of LMC clusters presented in Bica et al. (2008) has not yet been updated to reflect more recent cluster discoveries, we note that DELVE 2's position (depicted visually in Figure 1) places it outside the search regions for many recent efforts dedicated to searching for outer LMC satellites, including those conducted by DES (Pieres et al. 2016), the Optical Gravitational Lensing Experiment (OGLE; Sitek et al. 2016), and the YMCA (Yes, Magellanic Clouds Again) and STEP (The SMC in Time: Evolution of a Prototype interacting late-type dwarf galaxy) projects conducted on the VLT Survey Telescope (Gatto et al. 2020).

We proceed with  $g$ - and  $i$ -band tiling for further analysis of this candidate, as the effective exposure time and stellar PSFs for the  $i$ -band exposure at this location are better than the  $r$ -band exposure, which primarily resulted in more reliable star/galaxy separation. Since the  $r$  and  $i$  exposures are positioned identically on-sky, there is no difference in coverage between the two bands. While the initial detection significance was higher for the  $g$ ,  $r$  search, we found that the calculated test statistic (TS) from our parameter fit (Section 4) was higher when using the  $g$  and  $i$  bands. We note that the initial difference

in detection significance was due to a relatively poor determination of the distance modulus in the  $g$ - and  $i$ -band search, and we note that the Ultra-faint Galaxy Likelihood (*ugali*)–derived value of TS (see Section 4) is a far more robust indicator of the significance of the overdensity than the initial detection significance. Furthermore, we found that the best-fit parameters (including the TS) derived using the  $g$ - and  $r$ -band data were consistent within the stated uncertainties of the  $g$ - and  $i$ -band results presented in Section 4.

## 4. Properties of DELVE 2

In the following subsections, we characterize the morphology, stellar populations, distance, and proper motion of DELVE 2. We present the most probable values of these parameters with their associated uncertainties in Table 1.

### 4.1. Morphological and Isochrone Parameters

To fit the morphological and isochrone parameters of DELVE 2, we utilized the *ugali* software toolkit<sup>35</sup> (Bechtol et al. 2015; Drlica-Wagner et al. 2015), which uses an unbinned Poisson maximum-likelihood formalism to derive best-fit parameters and identify probable member stars for resolved stellar systems.<sup>36</sup> We modeled the spatial distribution of stars with a Plummer (1911) radial profile. We account for incomplete coverage near the system to avoid biasing the calculations of the stellar density profile. We flag  $n_{\text{side}} = 4096$  HEALPix pixels with no sources or limited observational coverage and exclude or down-weight them (respectively) when estimating the stellar density in each radial bin. Due to the compactness of this system and the complete coverage in its “core region,” this correction ultimately does not influence the profile fit significantly. A template Bressan et al. (2012) isochrone was fit to the observed color-magnitude diagram. We simultaneously fit the centroid R.A. and decl. ( $\alpha_{2000}$  and  $\delta_{2000}$ , respectively), extension along the semimajor axis ( $a_h$ ), ellipticity ( $\epsilon$ ), and position angle (P.A.) of the Plummer profile and the distance modulus ( $m - M$ ), age ( $\tau$ ), and metallicity ( $Z$ ) of the isochrone and derived the posterior

<sup>34</sup> Candidate clusters identified by OGLE in the SMC periphery and Magellanic bridge by Sitek et al. (2017) are included in the catalog of Bica et al. (2020).

<sup>35</sup> <https://github.com/DarkEnergySurvey/ugali>

<sup>36</sup> Appendix C of Drlica-Wagner et al. (2020) describes the statistical formalism implemented by *ugali*.

**Table 1**Morphological, Isochrone, and Proper-motion Parameters for DELVE 2 Based on the  $g$ - and  $i$ -band Data

Parameter	Value	Units
$\alpha_{2000}$	$28.772^{+0.006}_{-0.005}$	deg
$\delta_{2000}$	$-68.253^{+0.002}_{-0.002}$	deg
$\ell$	294.236	deg
$b$	-47.789	deg
$a_h$	$1.04^{+0.19}_{-0.15}$	arcmin
$r_h$	$1.02^{+0.18}_{-0.15}$	arcmin
$r_{1/2}$	$21^{+4}_{-4}$	pc
$\epsilon$	$0.03^{+0.15}_{-0.03}$	...
P.A.	$74^{+84}_{-40}$	deg
$m - M$	$19.26^{+0.03}_{-0.03} \pm 0.1^a$	mag
$D_\odot$	$71 \pm 4$	kpc
$\tau$	$> 13.3^b$	Gyr
$Z$	$0.00015^{+0.0001}_{-0.0001}$	...
$\sum_{ipi,ugali}$	$59^{+18}_{-10}$	...
TS	181	...
$M_V$	$-2.1^{+0.4c}_{-0.5}$	mag
$M_*$	$880^{+120d}_{-150}$	$M_\odot$
$\mu$	28.2	mag arcsec $^{-2}$
[Fe/H]	$-2.0^{+0.2e}_{-0.5}$	dex
$E(B - V)$	0.024	mag
$D_{GC}$	$69 \pm 4$	kpc
$\mu_\alpha \cos \delta$	$1.02^{+0.24}_{-0.25}$	mas yr $^{-1}$
$\mu_\delta$	$-0.85^{+0.18}_{-0.19}$	mas yr $^{-1}$
$\sum_{ipi,MM}$	$9.5^{+1.1}_{-0.3}$	...

**Notes.** Uncertainties were derived from the highest-density interval containing the peak and 68% of the marginalized posterior distribution.

<sup>a</sup> We assume a systematic uncertainty of  $\pm 0.1$  associated with isochrone modeling (Drlaca-Wagner et al. 2015).

<sup>b</sup> The age posterior peaks at the upper bound of the allowed parameter range (13.5 Gyr); thus, we quote a lower limit at the 84% confidence level.

<sup>c</sup> The uncertainty in  $M_V$  was calculated following Martin et al. (2008) and does not include uncertainty in the distance.

<sup>d</sup> We note that our estimate of  $M_*$  does not account for a mass contribution from possible blue straggler stars due to the difficulty of distinguishing them from the SMC foreground.

<sup>e</sup> Our estimate of [Fe/H] is derived from the best-fit PARSEC isochrone following the procedure described in Section 3 of Bressan et al. (2012) assuming a solar metallicity of  $Z_\odot = 0.0152$ .

probability distributions for each parameter using the affine-invariant Markov Chain Monte Carlo (MCMC) ensemble sampler, *emcee* (Foreman-Mackey et al. 2013). From these properties, we then derived estimates of the Galactic longitude and latitude ( $\ell$  and  $b$ , respectively), the azimuthally averaged angular and physical half-light radii ( $r_h$  and  $r_{1/2}$ , respectively), the average surface brightness within the half-light radius ( $\mu$ ), the heliocentric distance ( $D_\odot$ ), the 3D galactocentric distance ( $D_{GC}$ ) between DELVE 2 and the Galactic center (assumed to be  $D = 8.178$  kpc; Gravity Collaboration et al. 2019), the total stellar mass integrated along the best-fit isochrone ( $M_*$ ), the absolute integrated visual magnitude ( $M_V$ ), and the metallicity ([Fe/H]). The *ugali* membership probability ( $p_{ugali}$ ) of each star comes from the Poisson probability that a star belongs to DELVE 2 given its location relative to the best-fit spatial model, proximity to the best-fit isochrone in color-magnitude space, photometric measurement uncertainty, and local imaging depth. We calculated the sum of the *ugali* membership

probabilities across all stars,  $\sum_{ipi,ugali} = 59$ , indicating a significant number of likely member stars with  $g < 23.5$  mag.

In Figure 3, we plot the spatial distribution, color-magnitude diagram, and proper-motion vector-point diagram (see Section 4.2) for DELVE 2. In the left and middle panels, all stars with  $p_{ugali} > 0.05$  are colored by their *ugali* membership probability. In the middle panel, the derived best-fit PARSEC isochrone is drawn in black, and we circle stars identified as likely system members based on *Gaia* DR2 proper motions (shown in the right panel; see Section 4.2).

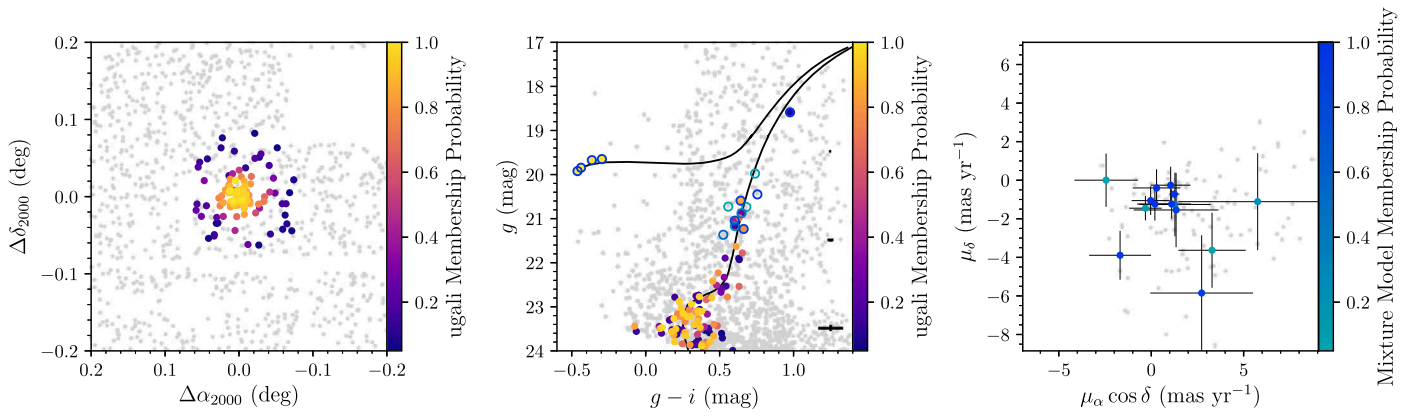
#### 4.2. Proper Motion

To verify the detection of DELVE 2 and measure the proper motion, we cross-matched stars within  $0.5^\circ$  of the system centroid with the *Gaia* DR2 catalog (Gaia Collaboration et al. 2018). The stellar sample was filtered by selecting stars consistent with zero parallax ( $\varpi - 4\sigma_\varpi \leq 0$ ), small proper motions (i.e., removing stars that would be unbound to the Milky Way if they were at the distance of DELVE 2), and a color-magnitude selection of 0.1 mag in  $g - i$  from a best-fit isochrone with metallicity [Fe/H] =  $-2.2$  and age  $\tau = 13.5$  Gyr.

To determine the proper motion of the satellite, we applied a Gaussian mixture model (Pace & Li 2019). Briefly, the mixture model separates the likelihoods of the satellite and the foreground stars, decomposing each into a product of spatial and proper-motion likelihoods. Stars that are closer to the centroid of the satellite are given higher weight based on the best-fit stellar distribution, and stars well outside the satellite help determine the Milky Way foreground proper-motion distribution. In contrast to Pace & Li (2019), we varied  $a_h$  and assumed a Gaussian prior based on the *ugali* results ( $a_h = 1.02 \pm 0.17$ ). The Pace & Li (2019) analysis used fixed the spatial parameters, which do not consider any uncertainty with the spatial distribution. We have also run the analysis with the spatial parameters fixed to their best-fit values and found that the results do not change appreciably. In addition, we utilized two components in the foreground population to model the LMC/SMC and Milky Way populations. The MultiNest algorithm (Feroz & Hobson 2008; Feroz et al. 2009) was used to determine the best-fit parameters, including the proper motions of the satellite and the Milky Way foreground stars. The mixture-model membership probability ( $p_{MM}$ ) of each star was calculated by taking the ratio of the satellite likelihood to the total likelihood from the posterior distribution (see Pace & Li 2019 for more details).

We derive a systemic proper motion of  $(\mu_\alpha \cos \delta, \mu_\delta) = (1.02^{+0.24}_{-0.25}, -0.85^{+0.18}_{-0.19})$  mas yr $^{-1}$ . In the right panel of Figure 3, we color candidate member stars with  $p_{MM} > 0.05$  by their mixture-model membership probability, and foreground stars with  $p_{MM} \leq 0.05$  are shown in gray. Stars cross-matched between the DELVE discovery and *Gaia* DR2 with  $p_{MM} > 0.05$  are outlined in the color-magnitude diagram in the central panel of Figure 3. We define the sum of the mixture-model membership probabilities as  $\sum_{ipi,MM}$  and find  $\sum_{ipi,MM} = 9.5^{+1.1}_{-0.3}$ . If we assume that DELVE 2 has a Chabrier (2001) initial mass function with an age of 13.5 Gyr and [Fe/H] of  $-2.2$ , then we predict that we should observe  $N = 4^{+3}_{-2}$  stars brighter than  $g \sim 21$  mag in *Gaia* based on 1000 *ugali* simulations. The difference between the (lower) predicted number of stars and the observed number is driven by the fact that the simulations predict a lower number on the





**Figure 3.** Spatial distribution map, color–magnitude diagram, and proper-motion plot for DELVE 2, with the former two colored by  $p_{\text{ugali}}$  and the latter colored by mixture-model membership probability ( $p_{\text{MM}}$ ). (Left) Spatial distribution of stars with  $g < 24.0$  and  $i < 23.5$  mag in a  $0.16 \text{ deg}^2$  area around the centroid of DELVE 2; possible member stars, defined as those with  $p_{\text{ugali}} > 0.05$ , are colored by their  $p_{\text{ugali}}$  membership probability. Stars with  $p_{\text{ugali}} \leq 0.05$  are shown in gray. (Middle) Color–magnitude diagram of the stars shown in the left panel, applying the same magnitude cuts. We include representative photometric error bars sampled at three different  $g$ -band magnitudes (19.5, 21.5, and 23.5 mag) in black. These error bars are positioned at an arbitrary location along the color axis. The best-fit PARSEC isochrone is drawn in black. Four blue horizontal-branch stars are identified as highly probable members of DELVE 2 and clustered very closely to the centroid of the system. Stars cross-matched with *Gaia* DR2 with  $p_{\text{MM}} > 0.05$  are outlined by their mixture-model membership probability. (Right) *Gaia* proper motions for stars cross-matched with the DELVE discovery data. Stars with  $p_{\text{MM}} > 0.05$  are colored by their mixture-model membership probability, and stars with  $p_{\text{MM}} \leq 0.05$  that pass an isochrone filter are shown in gray.

horizontal branch than the four stars we observe. In particular, the simulations predict  $2^{+1}_{-2}$  horizontal-branch stars with  $g - i < 0.35$  for the full horizontal branch and  $1 \pm 1$  blue horizontal-branch stars with  $g - i < 0$ . The latter result specifically should be compared with the observed four blue horizontal-branch stars.

We note that the  $p_{\text{ugali}}$  probabilities use color, magnitude, and spatial properties to determine membership probabilities, whereas the mixture model uses only proper motion and spatial properties to determine these probabilities (after a color–magnitude selection that is  $\sim 0.1 \text{ mag}$  wide in color has been applied). In particular, the  $p_{\text{ugali}}$  probabilities include a Chabrier (2001) IMF component, which down-weights the bright red giant branch stars with more precise proper motions. This results in some stars being identified as higher mixture-model probability proper-motion members but lower-probability  $p_{\text{ugali}}$  members.

#### 4.3. Checking for Known RR Lyrae Variable Stars

In an attempt to further constrain the distance to DELVE 2, we searched the OGLE (Soszyński et al. 2019) and *Gaia* (Clementini et al. 2019) catalogs for potential known RR Lyrae (RRL) variable stars associated with the system. These stars obey a well-constrained period–luminosity–metallicity relation, making them excellent standard candles for tracing the distances to old stellar populations, where they are often found. We found that there are seven and three RRL stars within  $1^\circ$  of DELVE 2 in the OGLE and *Gaia* catalogs, respectively. However, the closest RRL variable to DELVE 2 is  $\sim 21'$  away in projection (far beyond the maximum observed extent of the system), and all RRL stars are at closer heliocentric distances. Therefore, we conclude that these nearby RRL stars are consistent with either the foreground Milky Way stellar population or stars in the outskirts of the SMC and are not likely to be associated with DELVE 2. However, we note that all known Milky Way dwarf galaxy satellites fainter than  $M_V = -3.0$  have one or fewer known RRLs (Martínez-Vázquez et al. 2019); thus, the lack of known RRLs at the position of DELVE 2 is not particularly surprising, provided the system is a dwarf galaxy.

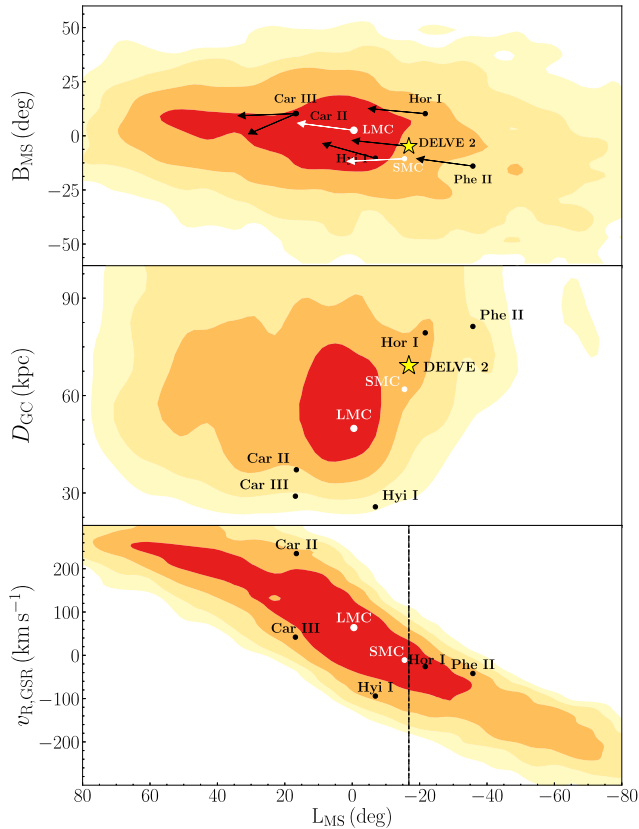
## 5. Discussion

In the previous sections, we have presented the discovery of DELVE 2 and characterized its morphological properties, stellar population, and systemic proper motion. In the following sections, we utilize this information to discuss DELVE 2’s potential association with the Magellanic Clouds and its classification as a stellar system.

### 5.1. Association with the Magellanic Clouds

The position of DELVE 2 in projection relative to the SMC and LMC ( $\sim 6.9^\circ$  and  $\sim 18.2^\circ$ , respectively) raises the immediate question of whether a physical association exists between the systems. We calculate the 3D separation between the centroid of DELVE 2 and the SMC,  $D_{\text{SMC}}$ , to be  $12.1^{+3.4}_{-2.8}$  kpc assuming  $(\alpha_{\text{SMC}}, \delta_{\text{SMC}}) = (13^\circ 18', -72^\circ 82')$  in celestial coordinates and an SMC distance of 61.94 kpc (de Grijs & Bono 2015). Similarly, we calculate the 3D separation between DELVE 2 and the LMC to be  $28.3^{+3.5}_{-3.3}$  kpc, assuming an LMC centroid of  $(\alpha_{\text{LMC}}, \delta_{\text{LMC}}) = (80^\circ 90', -68^\circ 74')$  (Wan et al. 2020) and an LMC distance of 49.89 kpc (de Grijs et al. 2014). This places the system beyond recent estimates for the tidal radius of the SMC (e.g., 5 kpc; Massana et al. 2020) and many recent estimates of the tidal radius of the LMC, for example,  $22.3 \pm 5.2$  kpc from van der Marel & Kallivayalil (2014). Thus, it is difficult to assess a priori whether the gravitational influence of the SMC or LMC is greater at the position of DELVE 2; we return to this issue in Section 5.2. These calculated separations, while fairly large compared to known star cluster satellites, preliminarily suggest an association with the Magellanic Cloud satellite system, which we explore further by considering the proper-motion signal detected in *Gaia* DR2.

To probe the relationship between DELVE 2 and the Magellanic Clouds, we compare the proper motion derived in Section 4.2 to the LMC infall models of Jethwa et al. (2016) in Figure 4. We plot the spatial position in Magellanic Stream coordinates (Nidever et al. 2008) of DELVE 2, the LMC, SMC, and five known ultra-faint galaxies suggested to be associated with the Magellanic system (Kallivayalil et al. 2018; Erkal & Belokurov 2020; Patel et al. 2020) over the numerically



**Figure 4.** Smoothed relative density of simulated LMC satellites from Jethwa et al. (2016), normalized to unity in each plot, displayed in Magellanic Stream coordinates. DELVE 2 is shown as a yellow star along with five likely LMC satellite galaxies (Hor I, Car II, Car III, Hyi I, and Phe II; Kallivayalil et al. 2018; Erkal & Belokurov 2020), shown as black circles. The LMC and SMC are shown as white circles. Note that Car II and Car III are spatially coincident in projection but have different proper-motion vectors, galactocentric distances, and velocities. (Top) Proper motion of the LMC, SMC, and five satellites. Arrows indicate the solar reflex-corrected proper motions of each system (no physical meaning is attributed to the magnitudes of these arrows). (Middle) Galactocentric distances ( $D_{GC}$ ) of the five likely LMC satellites and DELVE 2. (Bottom) Line-of-sight velocities in the Galactic standard of rest ( $v_{R,GSR}$ ) for five of the Magellanic dwarf galaxy satellites, in addition to the LMC and SMC. The black dashed line represents the MS longitude of DELVE 2.

simulated LMC tidal debris and visually highlight the direction of their solar reflex-corrected proper-motion vectors and that of DELVE 2. These five ultra-faint galaxies are Horologium I, Carina II, Carina III, Hydrus I, and Phoenix II, with proper-motion measurements coming from Kallivayalil et al. (2018) and Pace & Li (2019). While the classical dwarf galaxies Carina and Fornax have also been suggested to be LMC satellites (e.g., Pardy et al. 2020), we do not include them, since more detailed orbit modeling by Erkal & Belokurov (2020) and Patel et al. (2020) found that neither system is likely to be an LMC satellite.

As is visually apparent in the top panel of Figure 4, the proper motion of DELVE 2 is consistent with those of the LMC and SMC. DELVE 2 is trailing the Magellanic system, similar to the ultra-faint dwarfs Hor I and Phe II (as measured by Kallivayalil et al. 2018). DELVE 2 lies in a region with reasonably high simulated LMC satellite density, with a galactocentric distance between that of the SMC and Hor I. Based on the simulation data, we find that DELVE 2 is most likely to be associated with the Magellanic system if its line-of-

sight velocity in the Galactic standard of rest is within the range  $-80 \text{ km s}^{-1} \lesssim v_{R,GSR} \lesssim 50 \text{ km s}^{-1}$ . While a measurement of the line-of-sight velocity is required to confirm membership in the Magellanic system, we find it to be highly likely that DELVE 2 is a member based on the available data in comparison to simulations and known satellites.

As an additional check, we integrated the orbit of DELVE 2 backward in time to determine whether it was originally an LMC satellite as in Erkal & Belokurov (2020). In particular, we Monte Carlo sampled the present-day proper motions and distance 10,000 times from the values in this work. For each realization, we uniformly sampled the radial velocity between  $-500$  and  $500 \text{ km s}^{-1}$  and sampled the LMC’s radial velocity, distance, and proper motions from their observed values (van der Marel et al. 2002; Kallivayalil et al. 2013; Pietrzyński et al. 2013). The LMC was modeled as a Hernquist profile (Hernquist 1990) with a mass of  $1.5 \times 10^{11} M_{\odot}$  and a scale radius of 17.13 kpc (consistent with the results of Erkal et al. 2019). The Milky Way was modeled with a potential nearly identical to MWPotential2014 from Bovy (2015); the only difference was that the bulge was replaced with a Hernquist profile with a mass of  $5 \times 10^9 M_{\odot}$  and a scale radius of 0.5 kpc.

DELVE 2 was integrated backward in the combined presence of the Milky Way and LMC for 5 Gyr, significantly before the LMC’s accretion onto the Milky Way. At the end of the integration, we determined whether DELVE 2 was originally bound to the LMC. Given the 10,000 iterations, we then estimated the probability that it was bound as a function of radial velocity. We find a large range of radial velocities ( $-150 \text{ km s}^{-1} < v_{R,GSR} < 80 \text{ km s}^{-1}$ ) for which DELVE 2 has a  $>50\%$  chance of being an LMC satellite. The peak probability of 0.81 occurred at  $v_{R,GSR} \sim -5 \text{ km s}^{-1}$ . This result is broadly consistent with the predictions from the forward-modeled population of LMC satellites discussed above (i.e., Jethwa et al. 2016). Thus, DELVE 2 is a promising LMC satellite candidate, and future radial velocity measurements will likely be able to confirm its membership.

## 5.2. Tidal Disruption from the Magellanic Clouds?

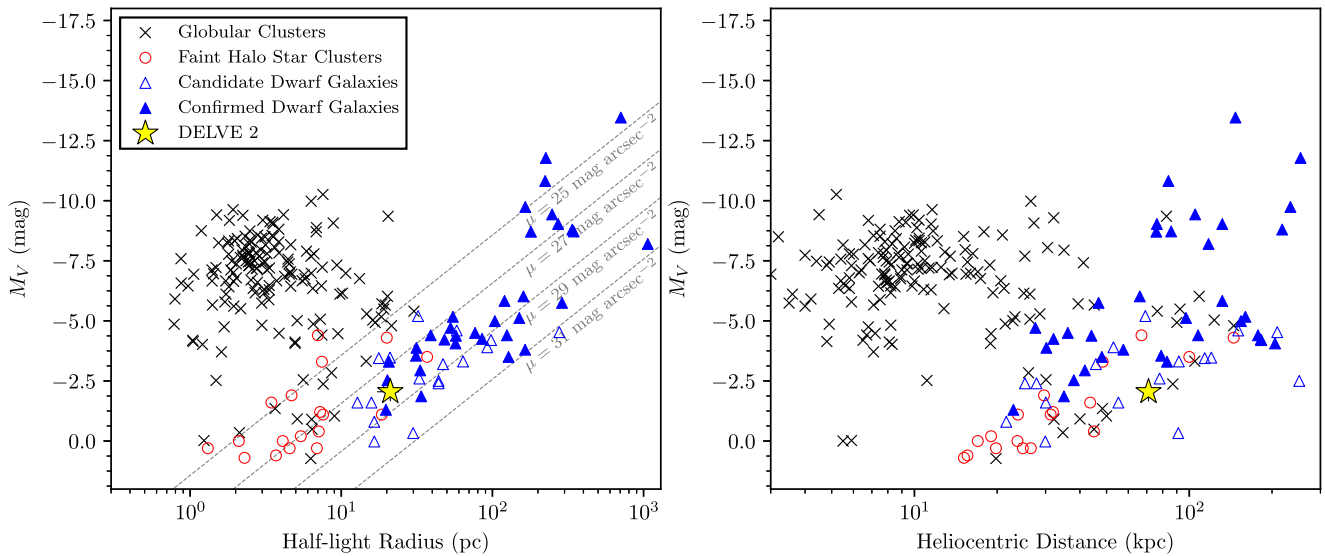
Given the relative proximity of DELVE 2 to the Magellanic Clouds, it is reasonable to explore whether the system might be undergoing tidal disruption due to the LMC, even if no obvious tidal features are visible in the spatial distribution of stars presented in Figure 3. To probe the survivability of DELVE 2 against the strong gravitational forces of the Magellanic system, we calculate its dynamical tidal radius ( $r_t$ ) due to the LMC following Equation (7) of Innanen et al. (1983), as applied in Martin et al. (2016),

$$r_t \simeq 0.5 \left( \frac{M_{\text{DELVE2}}}{M_{\text{LMC}}(D_{\text{LMC}})} \right)^{1/3} D_{\text{LMC}},$$

where  $D_{\text{LMC}}$  refers to the 3D separation between DELVE 2 and the LMC calculated above, and  $M_{\text{LMC}}(D_{\text{LMC}})$  is the enclosed mass of the LMC within a radius of  $D_{\text{LMC}}$ .

We find that whether or not DELVE 2 is undergoing tidal disruption from the LMC depends sensitively on its dynamical mass—a key determinant for the system’s classification as an ultra-faint galaxy or star cluster. In order for the dynamical tidal radius of DELVE 2 to be smaller than  $\sim 4.5 r_h$  ( $\sim 90 \text{ pc}$ ), corresponding to the maximum radius at which we find member stars identified with *ugali* membership probability greater than 5% ( $p_{\text{ugali}} > 0.05$ ), we calculate that the upper





**Figure 5.** (Left) Absolute magnitude vs. azimuthally averaged physical half-light radius for dwarf galaxy satellites of the Milky Way/LMC/SMC system (open and filled blue triangles for candidate and confirmed dwarf galaxies, respectively; Drlica-Wagner et al. 2020, and references therein), globular clusters (black crosses; Harris 1996), and recently discovered halo star clusters with  $D_\odot > 10$  kpc (red circles; Fadely et al. 2011; Muñoz et al. 2012; Balbinot et al. 2013; Belokurov et al. 2014; Laevens et al. 2014, 2015a; Kim & Jerjen 2015b; Kim et al. 2016; Luque et al. 2016, 2017, 2018; Koposov et al. 2017; Mau et al. 2019, 2020; Torrealba et al. 2019). DELVE 2 is displayed as a yellow star. Lines of constant surface brightness are drawn as diagonal dashed gray lines. (Right) Absolute magnitude vs. heliocentric distance of ultra-faint stellar systems in the Milky Way/LMC/SMC system. DELVE 2 occupies the ambiguous regime between recently discovered Milky Way halo star clusters and dwarf galaxies in this 3D parameter space.

bound on the system’s mass-to-light ratio must be  $M/L \lesssim 36$ , assuming a value of  $1.06 \times 10^{11} M_\odot$  as the LMC enclosed mass within 30 kpc (Wan et al. 2020), where this radius corresponds to the approximate 3D separation between DELVE 2 and the LMC.

Therefore, if DELVE 2 is found to be most consistent with the population of known ultra-faint dwarf galaxies, which are known to exhibit a wide range of (large) mass-to-light ratios ( $30 \lesssim M/L \lesssim 1000$ ; McConnachie 2012), we find that it is somewhat unlikely, but not impossible, that the system is undergoing tidal disruption due to the influence of the LMC. While a mass-to-light ratio of  $M/L \sim 36$  is not implausible with respect to the full Milky Way satellite galaxy population, this would be significantly lower than the mass-to-light ratio of the dwarf galaxy satellite Segue 1, which is of comparable absolute visual magnitude to DELVE 2 ( $M_V = -1.5^{+0.6}_{-0.8}$ ) but has  $M/L \sim 1320$  (Geha et al. 2009).<sup>37</sup>

In contrast, if DELVE 2 is found to have an  $M/L$  ratio consistent with the population of known star clusters, which typically exhibit mass-to-light ratios of  $M/L \sim 1$ –2 (Kruijsen 2008), we calculate a tidal radius for the system of  $r_t \lesssim 36$  pc. This upper bound lies at  $\sim 1.5 r_h$  for DELVE 2 and thus is well within the maximum system radius of  $\sim 4.5 r_h$ . In fact, approximately half of the stars with  $p_{\text{ugali}} > 0.05$  lie outside of this purported dynamical tidal radius. In this case, it would be almost certain that DELVE 2 is undergoing tidal disruption due to the LMC, provided its dynamical properties are found to be consistent with other recently discovered star clusters.

Repeating these calculations using the two SMC mass profiles specified in Table 4 of Patel et al. (2020), we find that

the influence of the SMC at the location of DELVE 2 is subdominant to that of the LMC. However, because all of the above calculations only account for the gravitational influence of either the LMC or the SMC alone at the position of DELVE 2, we would expect an even lower estimate of the dynamical tidal radius for the system (in both the cluster and dwarf galaxy cases) when including the influence of both simultaneously.

Evidence of tidal disruption (or lack thereof) could, in principle, be used to help discern whether or not DELVE 2 is a dark matter-dominated system. For example, Simon et al. (2017) utilized a similar argument and the observed tidal tails of the ultra-faint system Tucana III to constrain its mass-to-light ratio to be  $20 < M/L < 240$ , providing tentative evidence for a dark matter-dominated nature of the system, consistent with known dwarf galaxies. However, the lack of any clear morphological signatures of tidal disruption for DELVE 2 makes such a determination difficult based on the photometric and astrometric data alone, and the incomplete coverage near the system makes it impossible to conclusively state the absence of tidal disruption; thus, deeper and more complete imaging would be required to make a conclusion based on photometric properties alone. Additionally, spectroscopic follow-up may reveal tidal signatures beyond what photometric data alone can reveal, such as a velocity gradient; thus, conclusions about whether this system is undergoing tidal disruption/stripping or mass loss are best left until those data are available. However, we note that such an approach to the classification of this system could prove especially useful if DELVE 2 is found to have a mass low enough such that the velocity dispersion of the system cannot be resolved due to the systematics floor limiting current spectroscopic instruments, as was the case with Segue 2 (Kirby et al. 2013). We further discuss methods for the classification of DELVE 2 in the following subsection.

<sup>37</sup> While the Willman 1 system has a similar  $M_V$  to DELVE 2, the system’s dynamical state is unclear (Willman et al. 2011). Thus, the spectroscopically derived  $M/L$  ratio for that system may be unreliable and therefore is not ideal for comparison to DELVE 2.

### 5.3. Classification of DELVE 2

As is evident in Figure 5, DELVE 2 occupies a regime in the size–luminosity plane that makes it difficult to definitively classify the system as either an ultra-faint halo star cluster or a dwarf galaxy. The continuum between halo star clusters and ultra-faint dwarfs, roughly corresponding to  $M_V \gtrsim -2$  mag and  $10 \text{ pc} \lesssim r_{1/2} \lesssim 40 \text{ pc}$ , has been described in the literature as the “valley of ambiguity” or, similarly, the “trough of uncertainty” (e.g., Koposov et al. 2015b; Conn et al. 2018a, 2018b). While the system appears generally more consistent with the ultra-faint galaxy population, as viewed in Figure 5, few conclusions about the true nature of the system can be made in the absence of velocity and metallicity information.

In the absence of this information, comparing the morphological and photometric similarities of DELVE 2 to multiple other known systems offers some basic insight into its classification. In particular, DELVE 2 has a similar absolute magnitude to the ultra-faint dwarf galaxies Segue 1, Segue 2, Willman 1, Bootes II, and Carina III ( $M_V = -1.3$ ,  $-2.08$ ,  $-2.53$ ,  $-2.94$ , and  $-2.4$ , respectively; Muñoz et al. 2018; Torrealba et al. 2018). While these satellites are all slightly larger than DELVE 2 in terms of major-axis length ( $a_{1/2} = 24.2$ ,  $38.3$ ,  $27.7$ ,  $37.3$ , and  $30 \text{ pc}$ , respectively) and more elliptical ( $\epsilon = 0.33$ ,  $0.22$ ,  $0.47$ ,  $0.25$ , and  $0.55$ ), the azimuthally averaged radii of these systems are close to that of DELVE 2 ( $r_{1/2} = 19.8$ ,  $33.8$ ,  $20.2$ ,  $32.3$ , and  $20.1 \text{ pc}$ ).

The Milky Way halo star cluster with properties most similar to DELVE 2 (seen as a red circle directly below the gold star in Figure 5) is DES J0225+0304. This cluster system was likely tidally stripped from the Sagittarius dwarf galaxy (Luque et al. 2017); thus, the similarity between DELVE 2 and this system in terms of absolute magnitude and size may reflect analogous origins as stripped satellites of a larger galaxy accreting onto the Milky Way. Compared to the remaining population of Milky Way halo star clusters, DELVE 2 lies at a slightly fainter surface brightness,  $\mu = 28.2 \text{ mag arcsec}^{-2}$ , than most known systems. We compare DELVE 2 to the LMC/SMC cluster population in the following subsection.

Lastly, although not sufficient to make a conclusive judgment about the nature of stellar systems in isolation, the ellipticity of ultra-faint systems including DELVE 2 may also offer insight into their morphologies and dynamical states and thus can contribute to a broader case about their classifications. Compared to the known population of Milky Way ultra-faint satellite galaxies, DELVE 2 appears to stand out due to its unusually low ellipticity, even if the upper bound ellipticity of  $\epsilon < 0.18$  is considered. In general, globular clusters and their ultra-faint cluster analogs display lower ellipticity compared to their dwarf galaxy counterparts (e.g., Harris 1996; McConnachie 2012). While the projected distribution of stars appears to be well represented by our best-fit ellipticity, deep imaging of this system could provide a concrete assessment of photometric completeness and better disentangle member stars from foreground and background objects (e.g., Mutlu-Pakdil et al. 2018, 2019), allowing for a more reliable ellipticity estimate. We also note that this system’s major axis could be aligned with the line of sight, and thus it is possible that the system’s ellipticity is not well represented by the projected (2D) distribution of stars displayed in Figure 3.

Ultimately, the physical classification of DELVE 2 can best be made by measuring its stellar velocity dispersion and estimating its dynamical mass. A large velocity dispersion and derived mass-to-light ratio would suggest a dark matter–

dominated system, resulting in classification as a (probable) dwarf galaxy, while a smaller measured dispersion might suggest a lower dynamical mass and the absence of dark matter characteristic of the population of outer Milky Way star clusters (Simon 2019). Alternately, spectroscopic measurement of a large metallicity dispersion for DELVE 2 could imply the existence of multiple generations of star formation, resulting in a more probable classification of the system as an ultra-faint dwarf galaxy (Willman & Strader 2012).

We note that the four bright blue horizontal-branch stars and one bright red giant branch star with proper motions consistent with the systemic motion of DELVE 2 are accessible targets for future spectroscopic follow-up. In spite of these clear targets, the limited number of identifiable brighter red giant branch member stars available, the compactness of the central core of the system, and the possibility that the velocity dispersion for this (possibly low-mass) system may be at or below the systematic floor of current instruments may make the classification of this system challenging.

If DELVE 2 is confidently identified in follow-up studies as an ultra-faint dwarf galaxy, it should be referred to as Hydrus II, following the convention that ultra-faint dwarf galaxies are named after the constellation they reside in. Alternately, if DELVE 2’s properties prove to be most consistent with the population of recently discovered star clusters, the system should continue to be referred to as DELVE 2, following the convention that faint star clusters are named after the survey they are discovered in. Follow-up studies are needed to make a conclusion about the classification of DELVE 2, and its true nature remains unclear at this time.

### 5.4. Comparison to Known LMC/SMC Cluster Systems

Given the likelihood that DELVE 2 is associated with the Magellanic Clouds, it is worth probing the origins of this candidate system and its relationship to the known population of LMC/SMC star clusters.

The LMC is known to have brought a large population of star clusters as it has been accreted onto the Milky Way (Bica et al. 2008); thus, it is possible that DELVE 2 may share a similar history to the thousands of known star clusters in the Magellanic system. The LMC star cluster formation history is believed to be three-staged, including a period of rapid cluster star formation in the early universe ( $\tau \gtrsim 10 \text{ Gyr}$ ), followed by a long quiescent period between  $\sim 10$  and  $\sim 2\text{--}4 \text{ Gyr}$  ago and then by a period of rapid star cluster formation extending to the present day, potentially due to the interaction between the LMC and SMC (Harris & Zaritsky 2009; Weisz et al. 2013; Rubele et al. 2018; Ruiz-Lara et al. 2020). One consequence of this period of quiescence in the LMC cluster formation history is the so-called “age gap” in the age distribution of LMC clusters, with a small ( $N \lesssim 20$ ) population of globular clusters with ages comparable to most known Milky Way globular clusters, separated by the gap from a much larger population of less massive young clusters (e.g., Bertelli et al. 1992; Girardi et al. 1995; Olszewski et al. 1996). These two populations of clusters obey an overarching age–metallicity relation, within which the older clusters ( $\tau > 12 \text{ Gyr}$ ) are significantly more metal-poor ( $-2.2 \lesssim [\text{Fe}/\text{H}] \lesssim -1.2$ ) compared to the younger population of clusters ( $[\text{Fe}/\text{H}] \gtrsim -0.7$ ; Meschin et al. 2014).<sup>38</sup> Therefore,

<sup>38</sup> We note that Gatto et al. (2020) recently discovered 16 cluster candidates believed to be within the LMC cluster age gap ( $4 \text{ Gyr} \lesssim \tau \lesssim 10 \text{ Gyr}$ ).

although the photometrically derived metallicity and age for DELVE 2 are limited in accuracy by the small number of red giant branch stars available to precisely constrain these properties through synthetic isochrone fitting, it is clear that DELVE 2 is more consistent with an old, metal-poor stellar population and thus the former class of LMC clusters (provided the system is not a dwarf galaxy, as discussed in the previous subsection).

While the age and metallicity of DELVE 2 appear to be consistent with the older cluster population of the LMC described above, the position, absolute magnitude, and surface brightness differ significantly from the bright, massive “classical” globular clusters associated with the early epoch of LMC cluster formation (similar to those of the Milky Way; Figure 5). One potential explanation for the significant divergence between these old LMC star clusters and DELVE 2 could be that DELVE 2 originated as a more massive globular cluster associated with the early epoch of LMC star formation but has been tidally stripped over time due to tidal forces associated with the LMC’s interactions with the SMC in the last 4 Gyr.

Under this scenario, the observed system at present may be the remaining compact core of an older system, which would explain the apparent incompatibility of DELVE 2’s morphological properties with those of a Galactic/LMC globular cluster with similar age/metallicity. However, given its relatively large current distance from the LMC/SMC system (compared to known cluster systems), such extreme mass loss may only have been possible if DELVE 2’s orbit is highly elliptical, with a pericenter extremely close to the LMC or SMC. However, without radial velocity information or any visible signs of tidal disruption/mass loss in the current DELVE data, such a conclusion about DELVE 2’s orbital history is difficult to test.

In contrast to the conclusions reached above for the LMC, the old age of DELVE 2 appears inconsistent with the known population of SMC star clusters. Unlike the LMC, the SMC is known to host a population of globular clusters with an almost continuous distribution in age up to  $\tau \sim 8$  Gyr (e.g., Harris & Zaritsky 2004; Dias et al. 2010). Only one SMC cluster, NGC 121, serves as an exception to this distribution, with an age of  $\tau \sim 11$  Gyr, making the system the oldest known SMC cluster (Glatt et al. 2008). This system has a metallicity of  $[\text{Fe}/\text{H}] \sim -1.28$  (Dalessandro et al. 2016). While our metallicity and age estimates for DELVE 2 have fairly large uncertainties, the values we derived appear to be older and more metal-poor than NGC 121, currently accepted to be the only old, Milky Way-like globular cluster in the SMC (Glatt et al. 2008); thus, it is unlikely to have an SMC origin, unless this system is unique in its age/metallicity or represents a new class of previously undiscovered objects. With 6D motion information for this system, along with information about its chemical abundances, it may be possible in the future to probe these distinct theories for DELVE 2 and, in doing so, reach a comprehensive conclusion about the system’s origin, evolution, and classification.

## 6. Summary

We have presented the discovery of an ultra-faint resolved stellar system, DELVE 2, in a search of  $\sim 2200 \text{ deg}^2$  of early data from the DELVE survey in the Magellanic periphery, representing the third ultra-faint system discovered by the DELVE project to date. This new ultra-faint stellar system was

detected at high confidence by a search for spatial overdensities of stars consistent with an old, metal-poor stellar population. Based on maximum-likelihood fits to the system’s morphological and isochrone properties alone, we found that the system is consistent with an old, metal-poor stellar population, and by utilizing proper motions from *Gaia* DR2, we tentatively confirmed that DELVE 2 appears to be a gravitationally bound association of stars with coherent motion on the sky and found that the spatial position, distance, and proper motion strongly suggest an association between DELVE 2 and the LMC/SMC. However, we were unable to draw a robust conclusion about whether the system is more consistent with a dark matter-dominated dwarf galaxy or a faint star cluster. With three new satellites now identified by DELVE, and with numerical simulations predicting that  $\sim 100$  Milky Way satellites with  $M_V < 0 \text{ mag}$  and  $r_{1/2} > 10 \text{ pc}$  remain to be discovered (Nadler et al. 2020), we anticipate that DELVE will continue to play an important role in advancing our understanding of the Milky Way satellite system as the survey continues its comprehensive census of the southern sky.

W. C. acknowledges support from the University of Chicago Liew Family Research Fellowship. This work was supported in part by the U.S. Department of Energy, Office of Science, Office of Workforce Development for Teachers and Scientists (WDTS) under the Science Undergraduate Laboratory Internships (SULI) program. The DELVE project is partially supported by Fermilab LDRD project L2019-011 and the NASA Fermi Guest Investigator Program Cycle 9 No. 91201. A. B. P. acknowledges support from NSF grant AST-1813881. This research received support from the National Science Foundation (NSF) under grant No. NSF DGE-1656518 through the NSF Graduate Research Fellowship received by S.M. J. L. C. acknowledges support from NSF grant AST-1816196. J.D. S. acknowledges support from NSF grant AST-1714873. S. R. M. acknowledges support from NSF grant AST-1909497. D. M. D. acknowledges financial support from the State Agency for Research of the Spanish MCIU through the “Centre of Excellence Severo Ochoa” award for the Instituto de Astrofísica de Andalucía (SEV-2017-0709).

This project used data obtained with the Dark Energy Camera (DECam), which was constructed by the Dark Energy Survey (DES) collaboration. Funding for the DES Projects has been provided by the DOE and NSF (USA), MISE (Spain), STFC (UK), HEFCE (UK), NCSA (UIUC), KICP (U. Chicago), CCAPP (Ohio State), MIFPA (Texas A&M University), CNPQ, FAPERJ, FINEP (Brazil), MINECO (Spain), DFG (Germany), and the collaborating institutions in the Dark Energy Survey, which are Argonne Lab, UC Santa Cruz, University of Cambridge, CIEMAT-Madrid, University of Chicago, University College London, DES-Brazil Consortium, University of Edinburgh, ETH Zürich, Fermilab, University of Illinois, ICE (IEEC-CSIC), IFAE Barcelona, Lawrence Berkeley Lab, LMU München and the associated Excellence Cluster Universe, University of Michigan, NSF’s National Optical-Infrared Astronomy Research Laboratory, University of Nottingham, Ohio State University, OzDES Membership Consortium, University of Pennsylvania, University of Portsmouth, SLAC National Lab, Stanford University, University of Sussex, and Texas A&M University.

This work has made use of data from the European Space Agency (ESA) mission *Gaia* (<https://www.cosmos.esa.int/gaia>), processed by the *Gaia* Data Processing and Analysis



Consortium (DPAC; <https://www.cosmos.esa.int/web/gaia/dpac/consortium>). Funding for the DPAC has been provided by national institutions, in particular the institutions participating in the *Gaia* Multilateral Agreement.



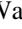
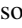







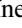

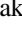



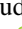



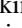

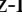



Based on observations at Cerro Tololo Inter-American Observatory, NSF's National Optical-Infrared Astronomy Research Laboratory (2019A-0305; PI: Drlica-Wagner), which is operated by the Association of Universities for Research in Astronomy (AURA) under a cooperative agreement with the National Science Foundation.





This manuscript has been authored by the Fermi Research Alliance, LLC, under contract No. DE-AC02-07CH11359 with the US Department of Energy, Office of Science, Office of High Energy Physics. The United States Government retains and the publisher, by accepting the article for publication, acknowledges that the United States Government retains a nonexclusive, paid-up, irrevocable, worldwide license to publish or reproduce the published form of this manuscript, or allow others to do so, for United States Government purposes.

*Facilities:* Blanco, *Gaia*.

*Software:* *astropy* (Astropy Collaboration et al. 2013; Price-Whelan et al. 2018), *emcee* (Foreman-Mackey et al. 2013), *fitsio*,<sup>39</sup> *HEALPix* (Górski et al. 2005),<sup>40</sup> *healpy*,<sup>41</sup> *Matplotlib* (Hunter 2007), *numpy* (Van Der Walt et al. 2011), *scipy* (Jones et al. 2001), *ugali* (Bechtol et al. 2015).<sup>42</sup>

## ORCID iDs

W. Cerny  <https://orcid.org/0000-0003-1697-7062>  
A. B. Pace  <https://orcid.org/0000-0002-6021-8760>  
A. Drlica-Wagner  <https://orcid.org/0000-0001-8251-933X>  
P. S. Ferguson  <https://orcid.org/0000-0001-6957-1627>  
S. Mau  <https://orcid.org/0000-0003-3519-4004>  
M. Adamów  <https://orcid.org/0000-0002-6904-359X>  
J. L. Carlin  <https://orcid.org/0000-0002-3936-9628>  
Y. Choi  <https://orcid.org/0000-0003-1680-1884>  
D. Erkal  <https://orcid.org/0000-0002-8448-5505>  
L. C. Johnson  <https://orcid.org/0000-0001-6421-0953>  
T. S. Li  <https://orcid.org/0000-0002-9110-6163>  
C. E. Martínez-Vázquez  <https://orcid.org/0000-0002-9144-7726>  
B. Mutlu-Pakdil  <https://orcid.org/0000-0001-9649-4815>  
D. L. Nidever  <https://orcid.org/0000-0002-1793-3689>  
K. A. G. Olsen  <https://orcid.org/0000-0002-7134-8296>  
A. Pieres  <https://orcid.org/0000-0001-9186-6042>  
E. J. Tollerud  <https://orcid.org/0000-0002-9599-310X>  
J. D. Simon  <https://orcid.org/0000-0002-4733-4994>  
A. K. Vivas  <https://orcid.org/0000-0003-4341-6172>  
D. J. James  <https://orcid.org/0000-0001-5160-4486>  
N. Kuropatkin  <https://orcid.org/0000-0003-2511-0946>  
S. Majewski  <https://orcid.org/0000-0003-2025-3147>  
D. Martínez-Delgado  <https://orcid.org/0000-0003-3835-2231>  
P. Massana  <https://orcid.org/0000-0002-8093-7471>  
E. H. Neilsen  <https://orcid.org/0000-0002-7357-0317>  
N. E. D. Noël  <https://orcid.org/0000-0002-8282-469X>  
A. H. Riley  <https://orcid.org/0000-0001-5805-5766>

D. J. Sand  <https://orcid.org/0000-0003-4102-380X>  
L. Santana-Silva  <https://orcid.org/0000-0003-3402-6164>  
G. S. Stringfellow  <https://orcid.org/0000-0003-1479-3059>  
D. L. Tucker  <https://orcid.org/0000-0001-7211-5729>

## References

- Astropy Collaboration, Robitaille, T. P., Tollerud, E. J., et al. 2013, *A&A*, **558**, A33
- Balbinot, E., Santiago, B. X., da Costa, L., et al. 2013, *ApJ*, **767**, 101
- Bechtol, K., Drlica-Wagner, A., Balbinot, E., et al. 2015, *ApJ*, **807**, 50
- Belokurov, V., Irwin, M. J., Koposov, S. E., et al. 2014, *MNRAS*, **441**, 2124
- Belokurov, V., Walker, M. G., Evans, N. W., et al. 2009, *MNRAS*, **397**, 1748
- Belokurov, V., Walker, M. G., Evans, N. W., et al. 2010, *ApJL*, **712**, L103
- Belokurov, V., Zucker, D. B., Evans, N. W., et al. 2006, *ApJL*, **647**, L111
- Belokurov, V., Zucker, D. B., Evans, N. W., et al. 2007, *ApJ*, **654**, 897
- Bernstein, G. M., Abbott, T. M. C., Armstrong, R., et al. 2018, *PASP*, **130**, 054501
- Bertelli, G., Mateo, M., Chiosi, C., & Bressan, A. 1992, *ApJ*, **388**, 400
- Bertin, E. 2011, in ASP Conf. Ser. 442, *Astronomical Data Analysis Software and Systems XX*, ed. I. N. Evans et al. (San Francisco, CA: ASP), 435
- Bertin, E., & Arnouts, S. 1996, *A&AS*, **117**, 393
- Bica, E., Bonatto, C., Dutra, C. M., & Santos, J. F. C. 2008, *MNRAS*, **389**, 678
- Bica, E., Westera, P., Kerber, L. d. O., et al. 2020, *AJ*, **159**, 82
- Bovy, J. 2015, *ApJS*, **216**, 29
- Bressan, A., Marigo, P., Girardi, L., et al. 2012, *MNRAS*, **427**, 127
- Burke, D. L., Rykoff, E. S., Allam, S., et al. 2018, *AJ*, **155**, 41
- Cannon, R. D., Hawarden, T. G., & Tritton, S. B. 1977, *MNRAS*, **180**, 81P
- Chabrier, G. 2001, *ApJ*, **554**, 1274
- Chambers, K. C., Magnier, E. A., Metcalfe, N., et al. 2016, arXiv:1612.05560
- Clementini, G., Ripepi, V., Molinaro, R., et al. 2019, *A&A*, **622**, A60
- Conn, B. C., Jerjen, H., Kim, D., & Schirmer, M. 2018a, *ApJ*, **852**, 68
- Conn, B. C., Jerjen, H., Kim, D., & Schirmer, M. 2018b, *ApJ*, **857**, 70
- Dalssandro, E., Lapenna, E., Mucciarelli, A., et al. 2016, *ApJ*, **829**, 77
- DES Collaboration, Abbott, T., Abdalla, F. B., et al. 2016, *MNRAS*, **460**, 1270
- DES Collaboration, Abbott, T., Aldering, G., et al. 2005, arXiv:astro-ph/0510346
- DES Collaboration, Abbott, T. M. C., Abdalla, F. B., et al. 2018, *ApJS*, **239**, 18
- D'Onghia, E., & Lake, G. 2008, *ApJL*, **686**, L61
- de Grijs, R., & Bono, G. 2015, *AJ*, **149**, 179
- de Grijs, R., Wicker, J. E., & Bono, G. 2014, *AJ*, **147**, 122
- Deason, A. J., Wetzel, A. R., Garrison-Kimmel, S., & Belokurov, V. 2015, *MNRAS*, **453**, 3568
- Desai, S., Armstrong, R., Mohr, J. J., et al. 2012, *ApJ*, **757**, 83
- Dias, B., Coelho, P., Barbay, B., Kerber, L., & Idiart, T. 2010, *A&A*, **520**, A85
- Dooley, G. A., Peter, A. H. G., Carlin, J. L., et al. 2017, *MNRAS*, **472**, 1060
- Drlica-Wagner, A., Bechtol, K., Allam, S., et al. 2016, *ApJL*, **833**, L5
- Drlica-Wagner, A., Bechtol, K., Mau, S., et al. 2020, *ApJ*, **893**, 47
- Drlica-Wagner, A., Bechtol, K., Rykoff, E. S., et al. 2015, *ApJ*, **813**, 109
- Erkal, D., Belokurov, V., Laporte, C. F. P., et al. 2019, *MNRAS*, **487**, 2685
- Erkal, D., & Belokurov, V. A. 2020, *MNRAS*, **495**, 2554
- Fadely, R., Willman, B., Geha, M., et al. 2011, *AJ*, **142**, 88
- Feroz, F., & Hobson, M. P. 2008, *MNRAS*, **384**, 449
- Feroz, F., Hobson, M. P., & Bridges, M. 2009, *MNRAS*, **398**, 1601
- Flaugher, B., Diehl, H. T., Honscheid, K., et al. 2015, *AJ*, **150**, 150
- Foreman-Mackey, D., Hogg, D. W., Lang, D., & Goodman, J. 2013, *PASP*, **125**, 306
- Fritz, T. K., Battaglia, G., Pawlowski, M. S., et al. 2018, *A&A*, **619**, A103
- Gaia Collaboration, Brown, A. G. A., Vallenari, A., et al. 2018, *A&A*, **616**, A1
- Gatto, M., Ripepi, V., Bellazzini, M., et al. 2020, *MNRAS*, **499**, 4114
- Geha, M., Willman, B., Simon, J. D., et al. 2009, *ApJ*, **692**, 1464
- Girardi, L., Chiosi, C., Bertelli, G., & Bressan, A. 1995, *A&A*, **298**, 87
- Glatt, K., Gallagher, J. S. I., Grebel, E. K., et al. 2008, *AJ*, **135**, 1106
- Górski, K. M., Hivon, E., Banday, A. J., et al. 2005, *ApJ*, **622**, 759
- Gravity Collaboration, Abuter, R., Amorim, A., et al. 2019, *A&A*, **625**, L10
- Harris, J., & Zaritsky, D. 2004, *AJ*, **127**, 1531
- Harris, J., & Zaritsky, D. 2009, *AJ*, **138**, 1243
- Harris, W. E. 1996, *AJ*, **112**, 1487
- Hernquist, L. 1990, *ApJ*, **356**, 359
- Homma, D., Chiba, M., Komiyama, Y., et al. 2019, *PASJ*, **71**, 94
- Homma, D., Chiba, M., Okamoto, S., et al. 2016, *ApJ*, **832**, 21
- Homma, D., Chiba, M., Okamoto, S., et al. 2018, *PASJ*, **70**, S18
- Hunter, J. D. 2007, *CSE*, **9**, 90
- Innanen, K. A., Harris, W. E., & Webbink, R. F. 1983, *AJ*, **88**, 338
- Jahn, E. D., Sales, L. V., Wetzel, A., et al. 2019, *MNRAS*, **489**, 5348

<sup>39</sup> <https://github.com/esheldon/fitsio>

<sup>40</sup> <http://healpix.sourceforge.net>

<sup>41</sup> <https://github.com/healpy/healpy>

<sup>42</sup> <https://github.com/DarkEnergySurvey/ugali>

- Jethwa, P., Erkal, D., & Belokurov, V. 2016, *MNRAS*, **461**, 2212
- Jethwa, P., Erkal, D., & Belokurov, V. 2018, *MNRAS*, **473**, 2060
- Jones, E., Oliphant, T., Peterson, P., et al. 2001, SciPy: Open Source Scientific Tools for Python, <http://www.scipy.org/>
- Kallivayalil, N., Sales, L. V., Zivick, P., et al. 2018, *ApJ*, **867**, 19
- Kallivayalil, N., van der Marel, R. P., Besla, G., Anderson, J., & Alcock, C. 2013, *ApJ*, **764**, 161
- Kim, D., & Jerjen, H. 2015a, *ApJL*, **808**, L39
- Kim, D., & Jerjen, H. 2015b, *ApJ*, **799**, 73
- Kim, D., Jerjen, H., Mackey, D., Da Costa, G. S., & Milone, A. P. 2016, *ApJ*, **820**, 119
- Kirby, E. N., Boylan-Kolchin, M., Cohen, J. G., et al. 2013, *ApJ*, **770**, 16
- Koposov, S. E., Belokurov, V., & Torrealba, G. 2017, *MNRAS*, **470**, 2702
- Koposov, S. E., Belokurov, V., Torrealba, G., & Evans, N. W. 2015a, *ApJ*, **805**, 130
- Koposov, S. E., Casey, A. R., Belokurov, V., et al. 2015b, *ApJ*, **811**, 62
- Koposov, S. E., Walker, M. G., Belokurov, V., et al. 2018, *MNRAS*, **479**, 5343
- Kruijssen, J. M. D. 2008, *A&A*, **486**, L21
- Laevens, B. P. M., Martin, N. F., Bernard, E. J., et al. 2015a, *ApJ*, **813**, 44
- Laevens, B. P. M., Martin, N. F., Ibata, R. A., et al. 2015b, *ApJL*, **802**, L18
- Laevens, B. P. M., Martin, N. F., Sesar, B., et al. 2014, *ApJL*, **786**, L3
- Luque, E., Pieres, A., Santiago, B., et al. 2017, *MNRAS*, **468**, 97
- Luque, E., Queiroz, A., Santiago, B., et al. 2016, *MNRAS*, **458**, 603
- Luque, E., Santiago, B., Pieres, A., et al. 2018, *MNRAS*, **478**, 2006
- Lynden-Bell, D. 1976, *MNRAS*, **174**, 695
- Martin, N. F., de Jong, J. T. A., & Rix, H.-W. 2008, *ApJ*, **684**, 1075
- Martin, N. F., Jungbluth, V., Nidever, D. L., et al. 2016, *ApJL*, **830**, L10
- Martin, N. F., Nidever, D. L., Besla, G., et al. 2015, *ApJL*, **804**, L5
- Martínez-Vázquez, C. E., Vivas, A. K., Gurevich, M., et al. 2019, *MNRAS*, **490**, 2183
- Massana, P., Noël, N. E. D., Nidever, D. L., et al. 2020, *MNRAS*, **498**, 1034
- Mau, S., Cerny, W., Pace, A. B., et al. 2020, *ApJ*, **890**, 136
- Mau, S., Drlica-Wagner, A., Bechtol, K., et al. 2019, *ApJ*, **875**, 154
- McConnachie, A. W. 2012, *AJ*, **144**, 4
- Meschin, I., Gallart, C., Aparicio, A., et al. 2014, *MNRAS*, **438**, 1067
- Morganson, E., Gruendl, R. A., Menanteau, F., et al. 2018, *PASP*, **130**, 074501
- Muñoz, R. R., Côté, P., Santana, F. A., et al. 2018, *ApJ*, **860**, 66
- Muñoz, R. R., Geha, M., Côté, P., et al. 2012, *ApJL*, **753**, L15
- Mutlu-Pakdil, B., Sand, D. J., Carlin, J. L., et al. 2018, *ApJ*, **863**, 25
- Mutlu-Pakdil, B., Sand, D. J., Walker, M. G., et al. 2019, *ApJ*, **885**, 53
- Nadler, E. O., Wechsler, R. H., Bechtol, K., et al. 2020, *ApJ*, **893**, 48
- Nidever, D. L., Majewski, S. R., & Butler Burton, W. 2008, *ApJ*, **679**, 432
- Nidever, D. L., Olsen, K., Walker, A. R., et al. 2017, *AJ*, **154**, 199
- Olszewski, E. W., Suntzeff, N. B., & Mateo, M. 1996, *ARA&A*, **34**, 511
- Pace, A. B., & Li, T. S. 2019, *ApJ*, **875**, 77
- Pardy, S. A., D’Onghia, E., Navarro, J., et al. 2020, *MNRAS*, **492**, 1543
- Patel, E., Kallivayalil, N., Garavito-Camargo, N., et al. 2020, *ApJ*, **893**, 121
- Pieres, A., Santiago, B., Balbinot, E., et al. 2016, *MNRAS*, **461**, 519
- Pietrzyński, G., Graczyk, D., Gieren, W., et al. 2013, *Natur*, **495**, 76
- Plummer, H. C. 1911, *MNRAS*, **71**, 460
- Price-Whelan, A. M., Sipőcz, B. M., Günther, H. M., et al. 2018, *AJ*, **156**, 123
- Rubele, S., Pastorelli, G., Girardi, L., et al. 2018, *MNRAS*, **478**, 5017
- Ruiz-Lara, T., Gallart, C., Monelli, M., et al. 2020, *A&A*, **639**, L3
- Sales, L. V., Navarro, J. F., Kallivayalil, N., & Frenk, C. S. 2017, *MNRAS*, **465**, 1879
- Schlafly, E. F., & Finkbeiner, D. P. 2011, *ApJ*, **737**, 103
- Schlegel, D. J., Finkbeiner, D. P., & Davis, M. 1998, *ApJ*, **500**, 525
- Sevilla-Noarbe, I., Bechtol, K., Carrasco Kind, M., et al. 2020, arXiv:2011.03407
- Simon, J. D. 2019, *ARA&A*, **57**, 375
- Simon, J. D., Li, T. S., Drlica-Wagner, A., et al. 2017, *ApJ*, **838**, 11
- Sitek, M., Szymański, M. K., Skowron, D. M., et al. 2016, *AcA*, **66**, 255
- Sitek, M., Szymański, M. K., Udalski, A., et al. 2017, *AcA*, **67**, 363
- Soszyński, I., Udalski, A., Szymański, M. K., et al. 2019, *AcA*, **69**, 87
- Tonry, J. L., Denneau, L., Flewelling, H., et al. 2018, *ApJ*, **867**, 105
- Torrealba, G., Belokurov, V., Koposov, S. E., et al. 2018, *MNRAS*, **475**, 5085
- Torrealba, G., Belokurov, V., Koposov, S. E., et al. 2019, *MNRAS*, **488**, 2743
- Torrealba, G., Koposov, S. E., Belokurov, V., & Irwin, M. 2016a, *MNRAS*, **459**, 2370
- Torrealba, G., Koposov, S. E., Belokurov, V., et al. 2016b, *MNRAS*, **463**, 712
- van der Marel, R. P., Alves, D. R., Hardy, E., & Suntzeff, N. B. 2002, *AJ*, **124**, 2639
- van der Marel, R. P., & Kallivayalil, N. 2014, *ApJ*, **781**, 121
- Van Der Walt, S., Colbert, S. C., & Varoquaux, G. 2011, *CSE*, **13**, 22
- Wan, Z., Guglielmo, M., Lewis, G. F., Mackey, D., & Ibata, R. A. 2020, *MNRAS*, **492**, 782
- Weisz, D. R., Dolphin, A. E., Skillman, E. D., et al. 2013, *MNRAS*, **431**, 364
- Wenger, M., Ochsenein, F., Egret, D., et al. 2000, *A&AS*, **143**, 9
- Willman, B., Blanton, M. R., West, A. A., et al. 2005a, *AJ*, **129**, 2692
- Willman, B., Dalcanton, J. J., Martínez-Delgado, D., et al. 2005b, *ApJL*, **626**, L85
- Willman, B., Geha, M., Strader, J., et al. 2011, *AJ*, **142**, 128
- Willman, B., & Strader, J. 2012, *AJ*, **144**, 76
- Wolf, C., Onken, C. A., Luvaul, L. C., et al. 2018, *PASA*, **35**, e010
- York, D. G., Adelman, J., Anderson, J. E., Jr., et al. 2000, *AJ*, **120**, 1579
- Zucker, D. B., Belokurov, V., Evans, N. W., et al. 2006a, *ApJL*, **650**, L41
- Zucker, D. B., Belokurov, V., Evans, N. W., et al. 2006b, *ApJL*, **643**, L103